Chart I

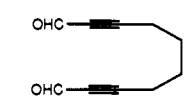

7

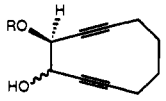

8 R = H
9 R = MMT

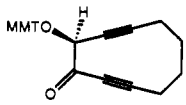

10

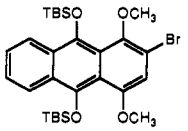

11

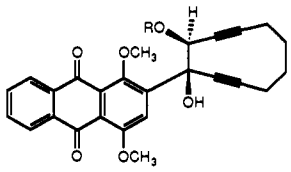

12 R = MMT
13 R = H

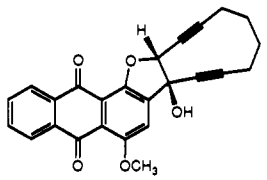

14

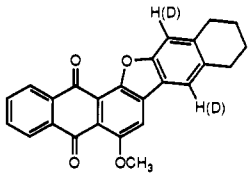

15

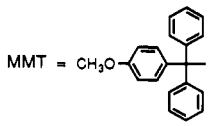

TBS = t-Bu(CH3)2Si

is removed by treatment of **12** with 0.1 N hydrochloric acid in 10% aqueous acetonitrile at 0 °C to produce the diol **13** (mp 135–136 °C) in 71% yield. Treatment of **13** with trifluoromethanesulfonic anhydride (2.0 equiv) and 2,6-lutidine (3.0 equiv) in dichloromethane at −78 °C forms the cyclic ether **14** (mp 124 °C dec) in 85% yield after purification on silica gel.[10] Transformation of **14** to the succinate ester **1** is accomplished by treatment of **14** with succinic anhydride (10 equiv), triethylamine (10 equiv), and DMAP (0.25 equiv) in dichloromethane for 2 h at 23 °C (83% yield, mp 115 °C dec). Succinate ester **1** is stable to routine handling and purification (silica gel chromatography) and is soluble in aqueous buffer solutions (pH 8.0) where control experiments establish that it is stable for at least several hours at 23 °C.

Reductive activation of **1** at pH 8.0 (0.1 M aqueous HEPES buffer, 23 °C) proceeds rapidly and cleanly with a flavin-based enzymatic system (ferredoxin reductase, glucose oxidase, isocitrate dehydrogenase, and catalase in the presence of glucose, NADPH, isocitrate, and $MnSO_4$, anaerobic incubation) to form the (*Z*)-enediyne **5** in 75% yield following extraction and flash column chromatography.[11] Control experiments show that ferredoxin reductase is the primary reductant; enediyne formation is slow in its absence and does not occur when both ferredoxin reductase and NADPH are omitted. NADPH alone induces clean formation of **5** from **1**, albeit more slowly than the enzyme-mediated reaction. The efficacy of this activation method is significant in that flavin-based enzymatic reductants have been implicated as potential in vivo activation factors for the clinically important quinone-containing antitumor agents mitomycin, adriamycin, and daunomycin.[3,11,12] As anticipated in light of ample precedent,[13] (*Z*)-enediyne **5** cyclizes slowly at 37 °C ($t_{1/2} \approx 2$ days) to form, in the presence of 1,4-cyclohexadiene, the aromatic product **15**.[14] Deuterium is incorporated quantitatively within the newly formed aromatic ring when the cyclization is conducted in THF-d_8, consistent with the intermediacy of biradical **6** in the transformation **5** → **15**.

In summary, we have demonstrated a new strategy for the generation of a reactive (*Z*)-enediyne by anthraquinone reductive activation in water. The efficiency of the enzymatic reduction system discussed above bodes well for potential in vivo activation of synthetic systems of this type.

Acknowledgment. Generous financial assistance from the National Institutes of Health and the David and Lucile Packard Foundation is gratefully acknowledged. P.S.D. acknowledges an ACS Division of Organic Chemistry Graduate Fellowship sponsored by the Procter & Gamble Company.

Supplementary Material Available: Reproductions of high-resolution ^{1}H NMR and IR spectral data for all synthetic intermediates (21 pages). Ordering information is given on any current masthead page.

(10) This product is believed to arise by nucleophilic displacement of the secondary triflate by methoxyl, followed by nucleophilic demethylation of the resulting oxonium ion. The corresponding secondary mesylate also forms **14** upon warming in DMF (70 °C).

(11) (a) Fisher, J.; Abdella, B. R. J.; McLane, K. E. *Biochemistry* **1985**, *24*, 3562. (b) Gutteridge, J. M. C.; Toeg, D. *FEBS Lett.* **1982**, *149*, 228.

(12) Reviews of anthracycline antibiotics: (a) *Anthracycline and Anthracenedione-Based Anticancer Agents*; Lown, J. W., Ed.; Elsevier: Amsterdam, 1988. (b) Fisher, J. F.; Aristoff, P. A. *Prog. Drug Res.* **1988**, *32*, 411.

(13) (a) Darby, N.; Kim, C. U.; Salaün, J. A.; Shelton, K. W.; Takada, S.; Masamune, S. *J. Chem. Soc., Chem. Commun.* **1971**, 1516. (b) Wong, H. N. C.; Sondheimer, F. *Tetrahedron Lett.* **1980**, *21*, 217. (c) Nicolaou, K. C.; Zuccarello, G.; Ogawa, Y.; Schweiger, E. J.; Kumazawa, T. *J. Am. Chem. Soc.* **1988**, *110*, 4866. (d) Nicolaou, K. C.; Hong, Y.-P.; Torisawa, Y.; Tsay, S.-C.; Dai, W.-M. *J. Am. Chem. Soc.* **1991**, *113*, 9878. See also ref 1f.

(14) Cyclization of **5** at 80 °C (2 M 1,4-cyclohexadiene, dimethylsulfoxide-d_6) proceeds with a half-life of ~20 min forming **15** in 75% yield.

Thermodynamically Controlled Electrochemical Formation of Thiolate Monolayers at Gold: Characterization and Comparison to Self-Assembled Analogs

Duane E. Weisshaar,† Brian D. Lamp, and Marc D. Porter*

Ames Laboratory-U. S. Department of Energy and Department of Chemistry, Iowa State University Ames, Iowa 50011

Received March 5, 1992

Thiolate monolayers self-assembled from dilute solutions of $X(CH_2)_nSH$ at gold[1] have emerged as attractive models of organic interfaces. We report herein the discovery of a new route for the preparation of thiolate monolayers that provides enhanced control of monolayer formation. The finding stems from our studies of the reductive desorption of these monolayers in alkaline solution via reaction 1.[2] We show that (1) the reverse of reaction 1 can

$$X(CH_2)_nSAu + e^- \rightarrow Au + X(CH_2)_nS^- \qquad (1)$$

be used for the electrodeposition of thiolate monolayers, (2) the electrodeposited monolayers have structures and interfacial

* Author to whom correspondence should be addressed.
† Permanent address: Department of Chemistry, Augustana College, Sioux Falls, SD 57197.

(1) For a general overview of self-assembled monolayers, see: (a) Ulman, A. *An Introduction to Ultrahigh Organic Films: From Langmuir-Blodgett to Self-Assembly*; Academic Press: Boston, 1991. (b) Whitesides, G. M.; Laibinis, P. E. *Langmuir* **1990**, *6*, 87–96.

(2) (a) Widrig, C. A.; Chung, C.; Porter, M. D. *J. Electroanal. Chem.* **1991**, *310*, 335–59. (b) Walczak, M. M.; Popenoe, D. D.; Deinhammer, R. S.; Lamp, B. D.; Chung, C.; Porter, M. D. *Langmuir* **1991**, *7*, 2687–93.

0002-7863/92/1514-5860$03.00/0

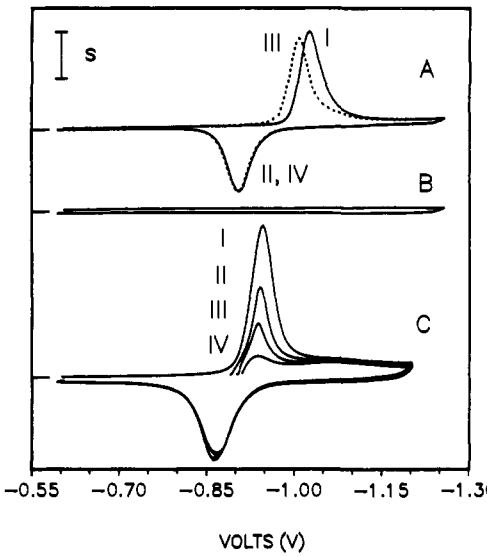

Figure 1. Cyclic voltammetric curves (uncorrected) for one-electron reductive desorption and oxidative deposition of thiolates at annealed, mica-supported gold. Conditions: 10 mM thiolate in 0.5 M ethanolic KOH, Ag/AgCl/saturated KCl reference electrode isolated by an aqueous KOH salt bridge, scan rate 100 mV/s. (A) Dodecanethiolate: I (solid line) desorption of self-assembled monolayer; II (solid line) electrodeposition of partial monolayer; III (dotted line) desorption of partial monolayer; IV (dotted line) subsequent electrodeposition of partial monolayer. (B) Uncoated gold in supporting electrolyte only. (C) Hexanethiolate (formation voltage): I (open circuit), II (−0.89 V), III (−0.90 V), and IV (−0.91 V). See text for experimental details for C. S is 50 μA in A and B and is 25 μA in C.

properties similar to those of their self-assembled analogs, and most importantly, (3) *the extent of deposition can be controlled by the reaction thermodynamics.*

The sequence of cyclic voltammetric curves in Figure 1A for 10 mM dodecanethiolate in 0.5 M ethanolic KOH demonstrates the electrodeposition process at annealed, mica-supported gold films.[3,4] The charge under curve I, which results from the desorption of a self-assembled monolayer, translates to a surface coverage of 8.9×10^{-10} mol/cm^2. Curve II, produced upon scan reversal, arises from the electrodeposition process. Both the coverage (8.1×10^{-10} mol/cm^2) determined from and position[5] of curve III (slightly positive of curve I) indicate the desorption of the partial monolayer that was formed on the oxidative scan (curve II). Coverages for monolayers deposited under these conditions (100 mV/s and 10 mM thiolate) are typically slightly less than a monolayer and are determined by deposition kinetics. A full monolayer can be formed by holding the applied voltage at a value positive of the deposition wave (e.g., −0.60 V) for >1 min. Voltammograms from continuous scanning are superimposable, demonstrating the reproducibility and reversibility of the deposition/desorption process. Coverages for electrodeposited and self-assembled monolayers vary ~10% from sample to sample, but only ~2% for electrodeposition at a given sample location.

The sharp, symmetrical shape of the oxidative peaks for dodecanethiolate (Figure 1A) and for hexanethiolate (Figure 1C) is diagnostic of a surface deposition process with a fast electron-transfer rate at this voltammetric time scale.[6] The large peak separations observed in Figure 1A,C largely reflect the contribution of the monolayer to the double-layer capacitance (C_{dl}),[2a] which leads to an increasing cathodic shift of the desorption wave with increasing chain length. Deposition/desorption of an ethanethiolate monolayer (not shown), where the contribution of the monolayer to C_{dl} is negligible, exhibits a peak separation of only 5 mV after correction for ~200 Ω of uncompensated solution resistance. This small peak separation is further evidence of a fast electron-transfer rate. Together, these findings suggest the possibility of controlling the extent of deposition by the reaction thermodynamics.

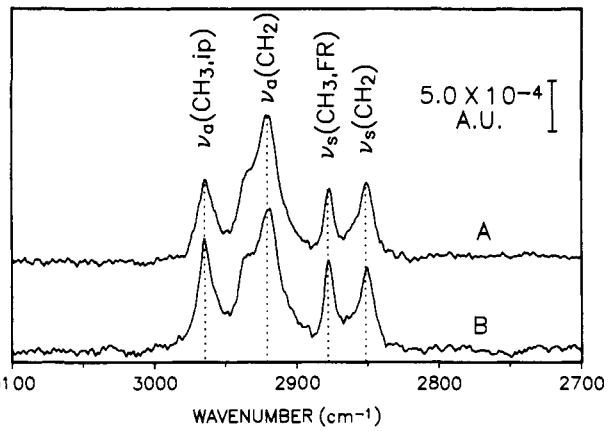

Figure 2. Infrared reflection spectra (2 cm^{-1} resolution) in the C–H stretching region for an electrodeposited (A) and a self-assembled (B) dodecanethiolate monolayer at gold.

The voltammetric curves in Figure 1C establish that controlled deposition of partial monolayers can be accomplished through voltage control (thermodynamics) instead of kinetic control. Here, the applied voltage is stepped from −1.2 V, where the thiolate is completely desorbed, to a preselected value on the anodic deposition wave for >1 min.[7] During this time, a redox equilibrium is established that produces a partial monolayer. The partial monolayer is then desorbed by a cathodic scan initiated at the applied voltage. Coverages for applied voltages of −0.89 (curve II), −0.90 (curve III), and −0.91 V (curve IV) correspond to 4.0×10^{-10}, 1.9×10^{-10}, and 0.80×10^{-10} mol/cm^2, respectively. Voltammetry for a self-assembled hexanethiolate monolayer (curve I, 8.2×10^{-10} mol/cm^2) is provided for comparison. Variability of coverage is within the uncertainties cited for the electrodeposition of full monolayers.

Finally, both contact angle and infrared reflection spectroscopic characterization[3] of full monolayers establish the qualitative similarities of the electrodeposited and self-assembled monolayers. Advancing contact angles (θ_a) of hexadecane (HD) and water at the two types of decanethiolate monolayers are effectively identical (electrodeposited: $\theta_a(H_2O) = 108°$, $\theta_a(HD) = 44°$; self-assembled:[8a] $\theta_a(H_2O) = 107°$, $\theta_a(HD) = 44°$). As shown in Figure 2, the absorbances and positions of the bands in the C–H stretching region of the infrared reflection spectra for an electrodeposited and a self-assembled monolayer of dodecanethiolate are comparable within preparative reproducibility. These similarities confirm that electrochemical deposition produces a monolayer of the ex-

(3) See ref 2a,b for preparative and other experimental details.

(4) The voltammetric deposition/desorption of thiolates at Si- and glass-supported gold films is more poorly defined (i.e., multiple waves) than at annealed, mica-supported gold films. We suspect this results from differences in the microscopic roughness on the three substrates, i.e., a much larger density of atomic steps on the Si- and glass-supported gold than on the annealed gold on mica (M. M. Walczak, B. D. Lamp, and M. D. Porter, unpublished results).

(5) Longer chain thiolate monolayers are more densely packed[8b] with small changes in coverage having a greater effect on C_{dl} than shorter chain monolayers. This results in a greater coverage-dependent variation in the desorption peak potential for the longer chain thiolate monolayers (compare Figure 1A,C).

(6) (a) Bard, A. J.; Faulkner, L. R. *Electrochemical Methods: Fundamentals and Applications*; Academic Press: Boston, 1980; Chapter 12. (b) Murray, R. W. In *Electroanalytical Chemistry: A Series of Advances*; Bard, A. J., Ed.; Marcel Dekker: New York, 1984; Vol. 13, pp 200–203. (c) Brown, J. P.; Anson, F. C. *Anal. Chem.* **1977**, *49*, 1589–95.

(7) The gradual delamination of gold from mica in alkaline solutions generally limits deposition times to <3 min. Such delamination has also been found by others for similarly prepared substrates (D. Buttry, University of Wyoming, and D. Johnson, Iowa State University, private communications).

(8) (a) Bain, C. D.; Troughton, E. G.; Tao, Y. T.; Evall, J.; Whitesides, G. M.; Nuzzo, R. G. *J. Am. Chem. Soc.* **1989**, *111*, 321–35. (b) Porter, M. D.; Bright, T. B.; Allara, D. L.; Chidsey, C. E. D. *J. Am. Chem. Soc.* **1987**, *109*, 3559–68. (c) Nuzzo, R. G.; Dubois, L. H.; Allara, D. L. *J. Am. Chem. Soc.* **1990**, *112*, 558–69. (d) Chidsey, C. E. D.; Loiacono, D. N. *Langmuir* **1990**, *6*, 682–91.

pected composition and spatial arrangement of a self-assembled monolayer (e.g., average polymethylene chain tilt of ~30° from the surface normal[8b-d]). Though not as extensively examined, we have also electrodeposited monolayers of other thiolates (i.e., n = 1–15 for X = CH_3, n = 2 for X = $CF_3(CF_2)_7$, n = 1, 2 for X = COOH, and n = 2, 3 for X = OH), demonstrating that the electrodeposition process is, indeed, a general route for the formation of thiolate monolayers.

Studies to characterize further the thermodyamics of the adsorption/desorption process are underway. We are also beginning to explore the application of electrodeposition for site-selective monolayer formation on multielement electrode arrays and for the formation of partial and mixed monolayers of known composition.

Acknowledgment. D.E.W. gratefully acknowledges sabbatical leave support from Augustana College, Sioux Falls, SD. M.D.P. expresses appreciation for a Dow Corning Assistant Professorship and an Alcoa Foundation Faculty Development Award. Helpful discussions with J. Zak and R. Deinhammer are also acknowledged as well as communication of preliminary findings by D. Bittry. Ames Laboratory is operated for the U. S. Department of Energy by Iowa State University under Contract No. W-7405-eng-82. This work was supported by the Summer Faculty Research Participation Program of the U.S.D.O.E. and by the Advanced Life Support Division of the NASA-Ames Research Center (Contract No. NAG2-722).

Chemically-Induced Aggregation, Budding, and Fusion in Giant Vesicles: Direct Observation by Light Microscopy

F. M. Menger* and N. Balachander

Department of Chemistry, Emory University
Atlanta, Georgia 30322

Received April 13, 1992

Albert Einstein once wrote that "the only apparatus necessary for observing Brownian motion is the microscope, and it need not even be a particularly good one".[1] A similar sentiment can be expressed for the topic of this paper, membrane motion. We describe herein a synthetic system[2] that undergoes a remarkable set of morphological events, all of them chemically-induced and all of them visible under the microscope.[3] These include aggregation, budding, and fusion.

Direct microscopic observation of membrane mechanics in biomimetic systems was made possible by Reeves and Dowben,[4] who first described the synthesis of giant vesicles in which a single bilayer surrounds a space as large as a living cell. In our experiments, we used $(C_{12}H_{25})_2N^+(CH_3)_2Br^-$, a cationic amphiphile (T_c = 17 °C) henceforth called DDAB. Giant vesicles (10–200 μm in diameter) were formed by soaking a thin DDAB film in 50 °C water for about an hour and then shaking for 4 s. Membrane properties were observed with a microscope (a good one as it happened): a Leitz Laborlux S equipped with phase-contrast and dark-field illumination.

Giant vesicles (200 μL of 10 mg DDAB/20 mL water) were placed within the confines of a washer cemented onto a microscopic slide. To begin an experiment, 100 μL of an additive was injected into the center of the vesicle solution, and the mixture was examined at a 320× magnification (Figure 1).

Figure 1A shows that low levels of Na_2SO_4 (1.0 mM) cause DDAB giant vesicles, initially isolated from one another, to aggregate over several minutes. No fusion occurs (as had been previously reported[5] for sulfate added to submicroscopic vesicles

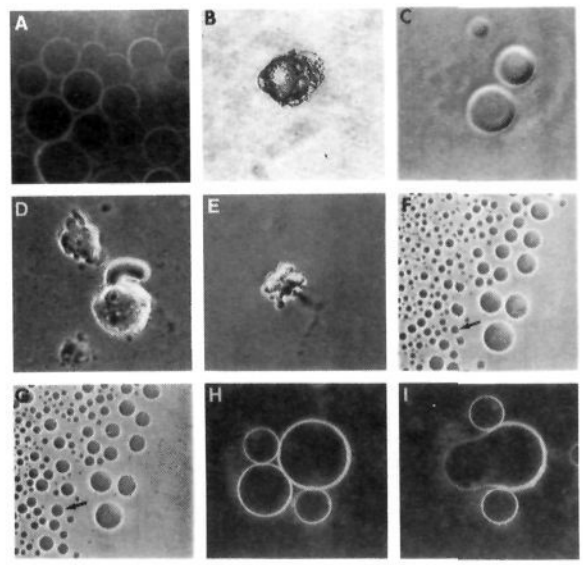

Figure 1. A: Aggregation of DDAB vesicles induced by sodium sulfate. Initially, only 3–4 vesicles were present in the microscopic field. B: Coagulation induced by sodium bromide. C: Flattening induced by equiosmolar glucose. D: Budding and vesicle ejection induced by sodium acetate. E: Continuation of the process seen in D in which all vesicles disappear to produce a clear microscopic field. F and G: Reappearance of vesicles after a few minutes. New vesicles fuse rapidly (compare vesicles indicated by arrows; photos F and G were taken less than 1 min apart). H and I: Dark-field photo of two fusing vesicles. Vesicles can sit side-by-side for many minutes, but fusion, once it begins, takes only seconds. Fused vesicles always reestablish a spherical shape (not shown). Experiments were carried out at 5–6 deg above the phase transition of the synthetic lipid. Additives were injected at a concentration of 0.1–0.3 M, except for the sodium sulfate which was used at a 1 mM concentration to avoid precipitation.

80 nm in diameter). High curvature clearly promotes the uniting of membranes. According to current dogma,[6] aggregation in the absence of fusion signifies that sulfate can neutralize long-range double-layer repulsion. On the other hand, sulfate apparently cannot subdue short-range "hydration repulsion" as would be necessary for fusion. Hydration forces reflect the need to desolvate headgroups prior to phase instability in the membrane.[7]

Injection of 0.1 M NaBr into the giant vesicle sample causes the DDAB to precipitate into a solid mass (Figure 1B). This is not purely an osmotic effect because equiosmolar glucose manages only to flatten the vesicles at the poles (Figure 1C). Salt-induced coagulation in submicroscopic vesicles is a well-studied phenomenon.[8]

Addition of NaOAc (0.1–0.3 M) leads to two striking effects: (a) the giant vesicles eject smaller vesicles by a budding process (Figure 1D,E). These small vesicles ultimately diminish in size and disappear to create a microscopically clear field. (b) After about 15 min, however, the field becomes speckled with newly formed vesicles that fuse at a prodigious rate (Figure 1F,G). The dark-field photos in Figure 1H,I catch two vesicles in the coupling act.

The acetate effect can be understood in terms of two notions: (a) strongly hydrated anions, such as acetate, bind relatively loosely to cationic surfaces,[9,10] and (b) according to the Svetina–Zeks model,[11] the coupled leaflets in a bilayer can act independently.

(1) Einstein, A.; Infield, L. *The Evolution of Physics*; Simon and Schuster: New York, 1966; p 59.
(2) Menger, F. M. *Angew. Chem., Int. Ed. Engl.* **1991**, *30*, 1086.
(3) Ringsdorf, H.; Schlarb, B.; Venzmer, J. *Angew. Chem., Int. Ed. Engl.* **1988**, *27*, 113.
(4) Reeves, J. P.; Dowben, R. M. *J. Cell Physiol.* **1969**, *73*, 49.
(5) Yogev, D.; Guillaume, B. C. R.; Fendler, J. H. *Langmuir* **1991**, *7*, 623.
(6) Hoekstra, D. *Biochemistry* **1982**, *21*, 2833.
(7) Cowley, A. C.; Fuller, N. L.; Rand, R. P.; Parsegian, V. A. *Biochemistry* **1978**, *17*, 3163. For an alternative viewpoint, see: Israelachvili, J. N.; Wennerström, H. *Langmuir* **1990**, *6*, 873.
(8) Carmona-Ribeiro, A. M.; Yoshida, L. S.; Chaimovich, H. *J. Phys. Chem.* **1985**, *89*, 2928.
(9) Underwood, A. L.; Anacker, E. W. *J. Colloid Interface Sci.* **1987**, *117*, 242. Anacker, E. W.; Underwood, A. L. *J. Phys. Chem.* **1981**, *85*, 2463.
(10) Evans, D. F. *Langmuir* **1988**, *4*, 3.
(11) Sackmann, E.; Duwe, H.-P.; Engelhardt, H. *Faraday Discuss. Chem. Soc.* **1986**, *81*, 281.

0002-7863/92/1514-5862$03.00/0